JOURNAL OF MATERIALS SCIENCE: MATERIALS IN MEDICINE 9 (1998) 429–437

# A comparison of the corrosion behaviour and surface characteristics of vacuum-brazed and heat-treated Ti6Al4V alloy

T. M. LEE, E. CHANG*
*Department of Materials Science and Engineering, National Cheng Kung University, Tainan, Taiwan*
*E-mail: n5882105@sparc1-cc.ncku.edu.tw*

C. Y. YANG
*Department of Orthopaedics, National Cheng Kung University Medical Centre, Tainan, Taiwan*

The corrosion characteristics of the brazed Ti6Al4V specimens were analysed and compared with respect to the conventionally heat-treated specimens by an electrochemical corrosion test. The object of this research was to explore the potentiality of the brazed titanium for biomaterials. The characteristics of the 1300 °C heat-treated and the 970 °C brazed specimens, with passivation and sterilization treatment, were evaluated by measurement of corrosion potential, $E_{corr}$, corrosion current densities, $I_{corr}$, polarization resistance of the reacted surface films, $R_p$, in a potentiodynamic test. The experimental results show that the corrosion rates of the heat-treated and the brazed samples are similar at $E_{corr}$, and the value of $E_{corr}$ for the brazed sample is noble to the heat-treated samples. The passive current density of the brazed specimen is either lower or higher than the heat-treated specimen, depending on the polarization potential. By Auger electron spectroscopic and high-resolution X-ray photoelectron spectroscopic analysis on specimens from the potentiostatic test, the elements of copper and nickel in the brazing filler were not detected while less alumina was found in the reacted film of the brazed specimens when compared with the heat-treated specimens. The implication of the results is discussed.

## 1. Introduction

The application of a porous coating on orthopaedic prosthesis has been practised for years. Because a porous-coated device has an increased surface area, the choice of better corrosion-resistant materials is important. Among the metals, titanium and titanium alloy have the merit of outstanding corrosion resistance, and useful combination of low density, low modulus of elasticity and high strength [1]. However, the mechanical properties of titanium substrate are seriously degraded by the sintered porous coating. In order to fabricate a porous-coated device suitable for bone ingrowth, Ti6Al4V alloy must be heat-treated above the beta transus of the material (992 °C) [2, 3]. Such a treatment results in a transformation from the equiaxed grain suggested for surgical implants, to lamellar alpha–beta microstructure. The lamellar alpha–beta structure has been shown to exhibit the worst fatigue properties of the most common structure attainable in Ti6Al4V alloy [2–5]. In addition, the bead–substrate neck zones will induce notch sensitivity which further decreases fatigue properties [2]. For solving the degradation of fatigue strength, Bugle [6] has suggested a diffusion-bonding method to manufacture the titanium-porous coating, and Crivella and Stouse [7] have adopted a joinder agent including cooper, with which the manufacturing temperature decreases to less than the beta transus.

In our previous study, the manufacture of a porous coating on Ti6Al4V alloy was applied by the vacuum brazing method [8]. In this method, a brazed filler with melting point below the beta transus was added between beads and substrate. The results revealed that the endurance limit of the brazing-coated Ti6Al4V alloy, tested under axial loading condition, was 215 MPa in comparison with 105 MPa for sintered material manufactured at 1300 °C. The increase in fatigue strength by the vacuum brazing method is thought to be due to (1) the microstructure effect in which the zone of lamellar alpha–beta structure at the beads/substrate interface was minimized and refined, and (2) the notch effect where the radius of curvature at the beads/substrate interface was much increased and became blunt, thus reducing the stress concentration.

* Author to whom all correspondence should be addressed.

0957–4530  

In this study, the corrosion characteristics of the 970 °C brazed specimens were analysed and compared with respect to the 1300 °C heat-treated specimens by an electrochemical corrosion test. The electrochemical properties of the brazed and the heat-treated specimens were evaluated by potentiodynamic polarization in Hank's solution. Meanwhile, potentiostatic measurements were taken to evaluate the reaction of brazed and heat-treated specimens under applied external potentials. The surface composition was detected by X-ray photoelectron spectroscopy (XPS) and Auger electron spectroscopy (AES). The objective of this research was to explore the potentiality of the brazed or low-melting-point titanium alloy for biomaterials.

## 2. Materials and methods

### 2.1. Experimental materials

The substrate used in this study was a surgical grade Ti6Al4V alloy (ASTM F136-92), and foil of Ti–15Cu–15Ni (wt %) with a melting point of 934 °C was selected as filler for the vacuum-brazing treatment. To prepare the brazed specimens, foils 0.05 mm thick were placed on 12.7 mm diameter × 2.0 mm Ti6Al4V alloy substrate and heat treated in a high-temperature furnace with a vacuum pressure less than $10^{-5}$ torr. The brazing cycle consisted of heating at 5 °C $min^{-1}$ to 970 °C, soaking for 2 to 8 h, followed by furnace cooling to room temperature. To simulate the conventionally sintered porous coatings, the Ti6Al4V alloy was plainly heat treated at 1300 °C for 2 h and was used as control for comparison with the brazed specimens; the heating rate and cooling conditions were the same as the brazing treatment. The three kinds of experimental material used in this study were (a) Ti6Al4V heat treated at 1300 °C for 2 h, (b) Ti6Al4V brazed at 970 °C for 2 h, and (c) Ti6Al4V brazed at 970 °C for 8 h. The heat-treated and brazed materials were ground through successive silicon carbide papers to 1500 grit, then subjected to sonication in acetone and rinsed three times in doubly distilled water. The experimental materials after polishing are denoted H, B2 and B8, respectively, in accordance with the prepared experimental materials, respectively.

### 2.2. Phase composition

The phase composition of the brazed specimens was detected by X-ray diffractometry (XRD, Rigaku D/max III. V) with a scan speed of 4° $min^{-1}$, using Cu$K_\alpha$ radiation (30 kV, 20 mA).

### 2.3. Surface chemical composition

Surface chemical analyses by EDS were carried out for the brazed samples. The samples were examined at 20 kV in a Jeol scanning electron microscope (model JSMR 840) equipped with energy dispersive spectroscopy (EDS, Link AN 1000/85S).

### 2.4. Potentiodynamic study

The heat-treated and brazed specimens were subsequently passivated in 34% $HNO_3$ for 1 h, and then sterilized in a steam autoclave at 121 °C for 30 min before potentiodynamic and potentiostatic testing. The passivated and sterilized specimens of the experimental H, B2 and B8 materials are denoted HP, B2P and B8P, respectively. The passivated specimens were placed into the aerated Hank's solution (Table 1) at 37 ± 1 °C and were equilibrated in the test solution for 1 h prior to generating polarization curves. The beginning potential was set at 200 mV active to the rest potential and the scan rate was 0.2 mV $min^{-1}$ in the noble direction.

### 2.5. Potentiostatic study and surface analysis

For potentiostatic study, specimens subjected to passivation and sterilization were immersed in the aerated Hank's solution for 2 h, under the applied potential voltages of $E_{corr}$, 1.0, 2.0 and 3.5 V (with reference to SCE). The current density of the tested specimens was recorded as a function of time. After the potentiostatic test, the surface morphology of the tested specimens was observed by scanning electron microscopy (SEM, Jeol JSMR 840), and the surface composition of the reacted surface film was examined by Auger electron spectroscopy (VG Microlab 310D). The vacuum pressure of the Auger electron spectroscope was $2.9 \times 10^{-9}$ mm Hg, and a monoenergetic electron beam with energy of 10 kV and current of 100 nA was employed. Selected specimens for depth-profile examination were milled by argon-ion bombardment at 3 kV and 9 mA.

X-ray photoelectron spectroscopy (XPS) was also carried out for measuring species of the nano-order reacted surface films. All analyses were carried out using the VG Scientific ESCALAB 210 (analysed area 0.5 mm diameter), operated at a chamber pressure less than $10^{-8}$ mbar, using Mg$K_\alpha$ radiation. The source was run at 12 kV and 20 mA from the magnesium anode. Measurements were made at a "take-off" angle 45° with respect to the sample surface. Survey spectra were recorded for all samples in the binding energy range 0–1000 eV. High-resolution scans of all samples were performed on titanium, aluminium, vanadium, copper, nickel and oxygen peaks. The binding energy scale was calibrated by the C 1s peak at 284.6 eV.

TABLE I Chemical compositions of Hank's solution

| Reagent | Composition ($g l^{-1}$) |
|---|---|
| NaCl | 8.0 |
| $CaCl_2$ | 0.14 |
| KCL | 0.4 |
| $NaHCO_3$ | 0.35 |
| Glucose | 1.0 |
| $MgCl_2 \cdot 6H_2O$ | 0.1 |
| $Na_2HPO_4 \cdot 2H_2O$ | 0.06 |
| $KH_2PO_4$ | 0.06 |
| $MgSO_4 \cdot 7H_2O$ | 0.06 |

## 3. Results

XRD patterns of the brazed specimens are shown in Fig. 1, which shows that the main peak is alpha-titanium structure and $Ti_2Cu$ exists as a minor phase. The amount of $Ti_2Cu$ decreases on increasing the period of brazing treatment from 2 h to 8 h.

EDS analyses of the chemical composition for the experimental materials are presented in Table II. Compared with Ti6Al4V, the 2 h brazed specimen shows a lower chemical composition (wt %) of aluminium, vanadium, with some additional copper and nickel elements. Brazing for the longer time of 8 h results in a reduction of copper and nickel contents compared to 2 h brazing treatment.

The results of the eletrochemical corrosion analyses for the passivated and sterilized specimens are shown in Fig. 2. The tafel extrapolation of polarization curve was adopted to measure the corrosion potential, $E_{corr}$, corrosion current densities, $I_{corr}$, and polarization resistance, $R_p$. A summary of the corrosion data for passivated and sterilized specimens is provided in Table III. The values of $E_{corr}$ are $-326.9$ mV (SCE) for 1300 °C treatment, $-191.6$ mV (SCE) for 2 h brazing treatment and $-210.6$ mV (SCE) for 8 h brazing treatment. The values of $I_{corr}$ are 6.983 nA $cm^{-2}$ for 1300 °C treatment, 7.988 nA $cm^{-2}$ for 2 h brazing treatment and 7.632 nA $cm^{-2}$ for 8 h brazing treatment. The values of $R_p$ are 4.428 MΩ $cm^{-2}$ for 1300 °C treatment, 3.918 MΩ $cm^{-2}$ for 2 h brazing treatment and 4.049 MΩ $cm^{-2}$ for 8 h brazing treatment. The polarization curves are similar between 2 and 8 h brazed specimens, and the current densities of the brazed specimens at 3.5 V (SCE) do not exceed $10^3$ μA $cm^{-2}$ (Fig. 2).

Fig. 3 shows the variation of current density as a function of time of passivated and sterilized specimens under the applied potential of 1.0 V (SCE) in the potentiostatic study. As shown in Fig. 3, the current densities for both the heat-treated and brazed specimens decrease upto 400 s and remain steady after that period. The values of current density in the steady state are 2.6 μA $cm^{-2}$ for the heat-treated specimens and 1.1 μA $cm^{-2}$ for the 2 h brazed specimens. For 2.0 V (SCE) and 3.5 V (SCE) applied potential voltages, the current-density curves of the heat treated and the brazed specimens are similar to the curves under the potential of 1.0 V (SCE). When the applied potential voltage is 2.0 V (SCE), the values of current density in the steady state are 10.21 μA $cm^{-2}$ for the heat-treated specimen and 136.6 μA $cm^{-2}$ for the 2 h brazed specimen. When the applied potential voltage is 3.5 V (SCE), the values of current density in the steady state are 259.1 μA $cm^{-2}$ for the heat-treated specimens and 567.3 μA $cm^{-2}$ for the 2 h brazed specimens. In addition, the current densities of the heat-treated and the brazed specimens are too low to be detected by the instrument when the external potential voltage is $E_{corr}$.

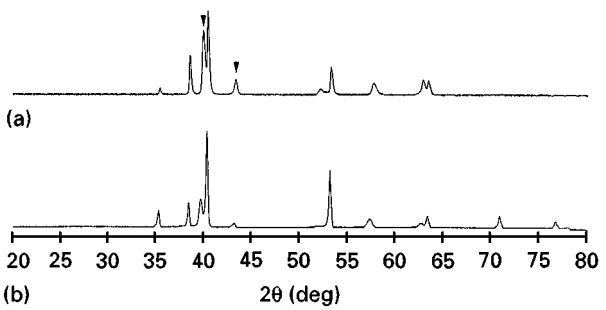


*Figure 1* XRD patterns of (a) B2 and (b) B8 specimens: (▼) $Ti_2Cu$.

TABLE II EDS analyses of surface chemical composition (wt %) for the H, B2 and B8 samples

| Materials | Ti | Al | V | Cu | Ni |
|---|---|---|---|---|---|
| H[a] | 90.0 | 6.0 | 4.0 | – | – |
| B2 | 85.28 | 2.81 | 2.01 | 4.45 | 5.45 |
| B8 | 86.72 | 3.33 | 2.65 | 3.58 | 3.72 |

[a] Nominal

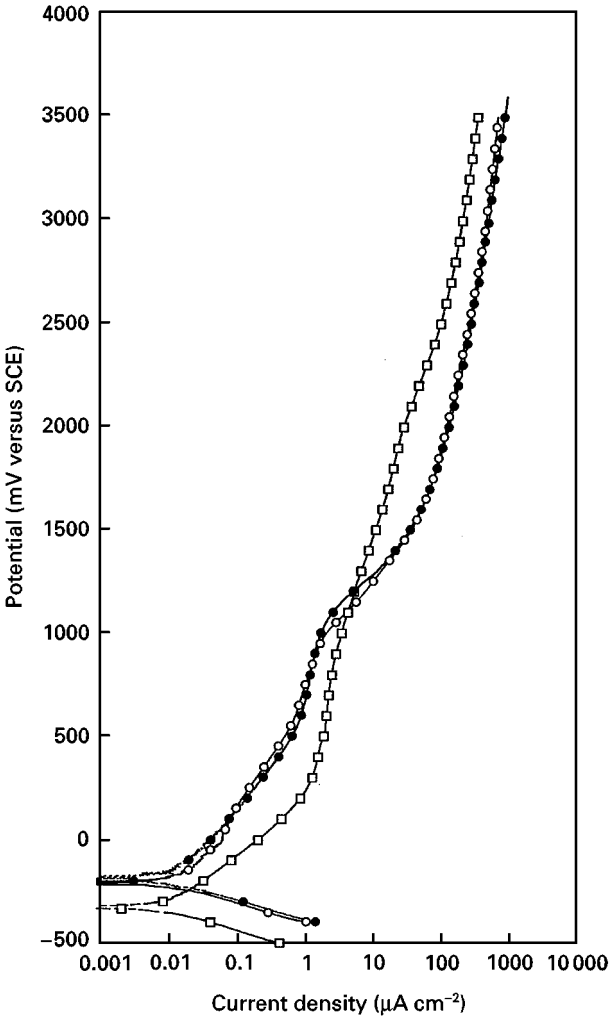


*Figure 2* Polarization curves of passivated and sterilized specimens: (□) HP, (●) B2P, (○) B8P.

TABLE III Corrosion characteristics of passivated and sterilized specimens

| | $E_{corr}$ (mV) versus SCE | $I_{corr}$ (nA $cm^{-2}$) | $R_P$ (MΩ $cm^{-2}$) |
|---|---|---|---|
| HP | – 326.9 | 6.983 | 4.428 |
| B2P | – 191.6 | 7.988 | 3.918 |
| B8P | – 210.6 | 7.632 | 4.049 |

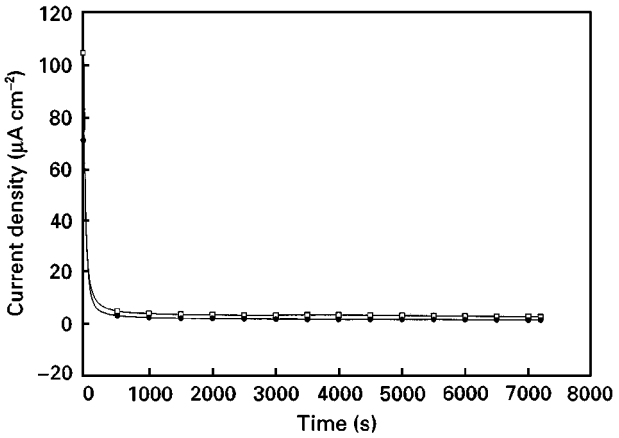


*Figure 3* Variation of current density as a function of time of passivated and sterilized specimens under the applied potential voltages of 1.0 V (SCE) in the potentiostatic test: (□) HP, (●) B2P.

Fig. 4 shows the broad-range XPS spectra of the heat-treated samples under four different potential voltages, and in this figure, titanium, aluminium, oxygen, carbon, sodium, calcium, nitrogen and sulphur are observed. Fig. 5 shows the broad-range XPS spectra of the 2 h brazed samples under four different potential voltages, and in this figure, titanium, aluminium, oxygen, carbon, sodium, calcium, nitrogen and sulfur are also observed, but the peaks of copper and nickel are not detected. By a more sensitive scale, copper and nickel are still not found in the surfaces of 2 h brazed samples applied by all potential voltages; the high-resolution XPS spectra of Cu 2p and Ni 2p at 1.0 V (SCE) are shown in Figs 6 and 7, respectively.

The high-resolution XPS spectra of Ti 2p of the heat-treated samples under four different potential voltages are shown in Fig. 8, in which the predominant oxide phase is $TiO_2$, and the various suboxide phases ($Ti^{2+}$ and $Ti^{3+}$) and metallic titanium are seen in the spectra. As shown in Fig. 8a, a higher content of $Ti^{2+}$ and $Ti^{3+}$ is found on the surface of the heat-treated sample applied by $E_{corr}$, but lower contents of $Ti^{2+}$ and $Ti^{3+}$ are found in specimens applied by 1.0 V (SCE), 2.0 V (SCE), and 3.5 V (SCE). The high-resolution XPS spectra of Ti 2p of the 2 h brazed samples applied by four different potential voltages are shown in Fig. 9, in which the predominant oxide phase is $TiO_2$, and the various suboxide phases ($Ti^{2+}$ and $Ti^{3+}$) and metallic titanium are also seen in the spectra. Similar relative contents of $Ti^{4+}$ to suboxides ($Ti^{2+}$ and $Ti^{3+}$) are found for the heat-treated and the brazed samples under the same applied potentials by comparing Figs 8 and 9.

Fig. 10 shows the results of AES depth-profile chemical compositions of the top surface of the heat-treated specimens subjected to $E_{corr}$ potential voltage. As shown in Fig. 10, the outer phase of the reacted film is composed of titanium, oxygen and aluminium, but the signal of vanadium is found after 500 s sputtering. Similarly, vanadium is also found in the inner phase for samples applied by 1.0 V (SCE), 2.0 V (SCE), and 3.5 V (SCE). The oxygen signal decreases to zero after 1400 s sputtering in the heat-treated specimens applied by $E_{corr}$ potential voltage, while the signals decrease to zero after 2000, 5000 and 7000 s sputtering in the heat-treated specimens subjected to 1.0 V (SCE), 2.0 V (SCE), and 3.5 V (SCE), respectively. Thus,

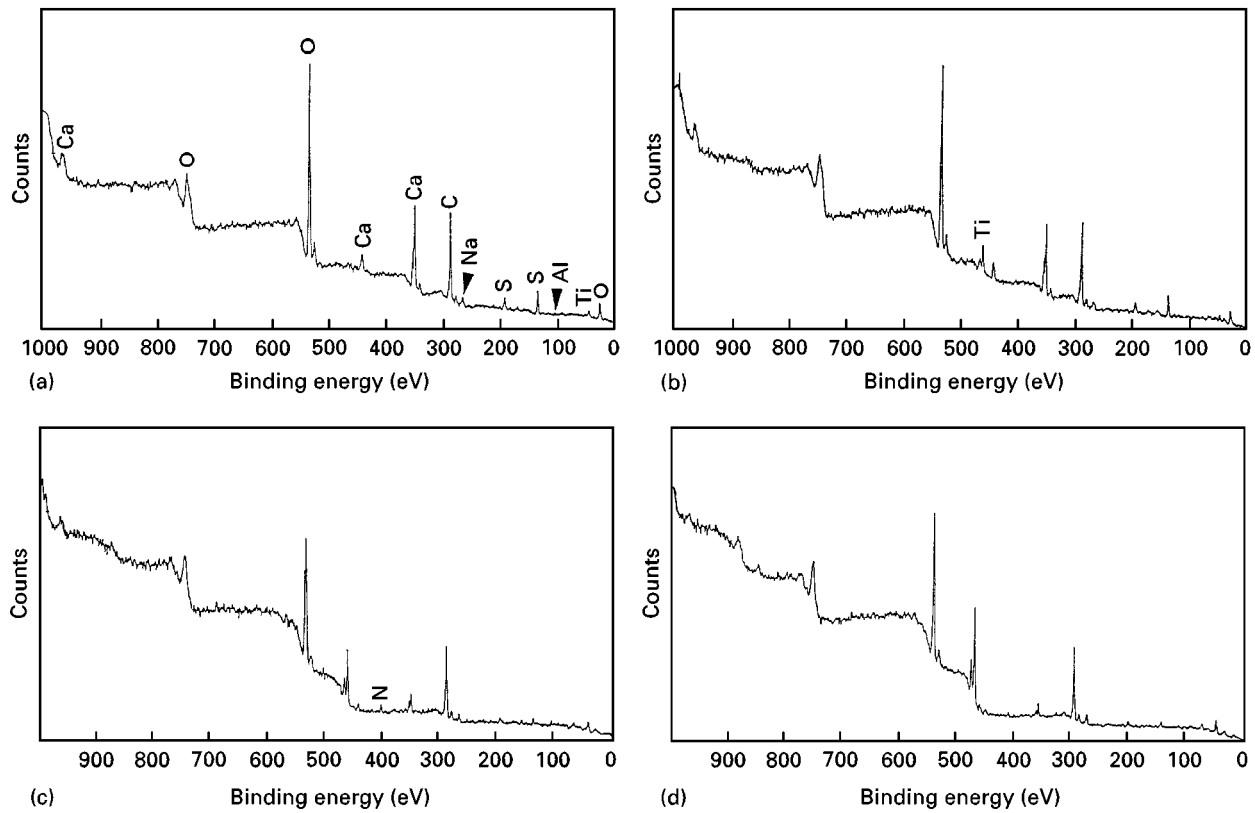


*Figure 4* Broad-range XPS spectra of HP samples under the applied potential of (a) $E_{corr}$, (b) 1.0 V (SCE), (c) 2.0 V (SCE), and (d) 3.5 V (SCE) in the potentiostatic test.

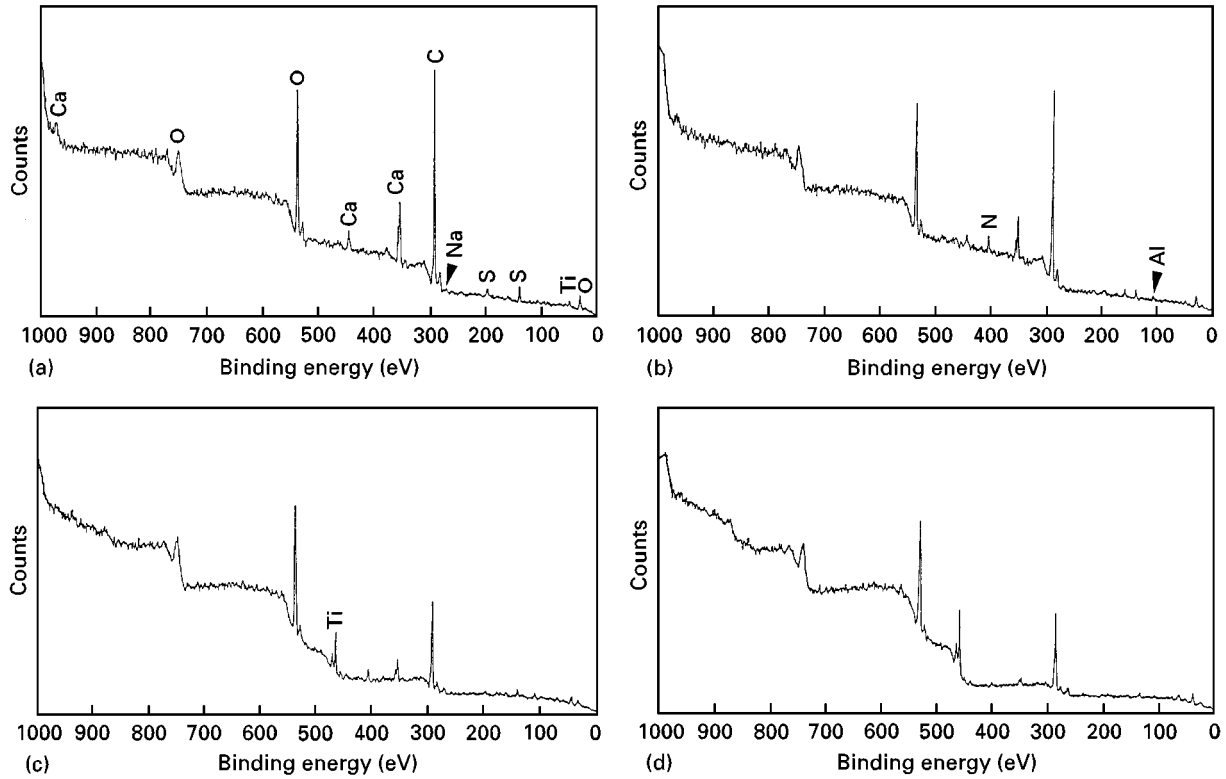


*Figure 5* Broad-range XPS spectra of B2P samples under the applied potential of (a) $E_{corr}$, (b) 1.0 V (SCE), (c) 2.0 V (SCE), and (d) 3.5 V (SCE) in the potentiostatic test.

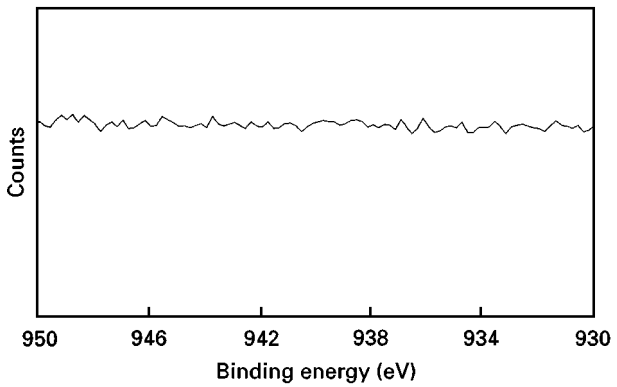


*Figure 6* High-resolution XPS spectrum of B2P sample under the applied potential of 1.0 V (SCE) in potentiostatic study. The result indicates the absence of copper (935 eV) in the spectrum.

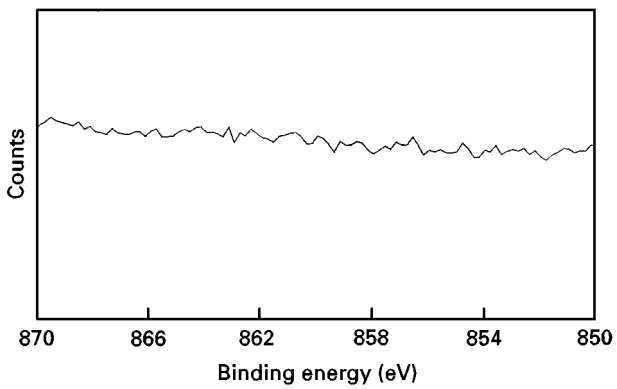


*Figure 7* High-resolution XPS spectrum of B2P sample under the applied potential of 1.0 V (SCE) in potentiostatic study. The result indicates the absence of nickel (852 eV) in the spectrum.

a thicker titanium oxide has been formed on the surface of the specimens at higher applied potential voltages.

Fig. 11 shows the results of AES depth-profile chemical compositions of top surface of the 2 h brazed specimen after $E_{corr}$ potential voltage is applied. Fig. 12 shows the AES spectrum of 500 s sputtered B2P specimens subjected to $E_{corr}$ potential; it can be seen that oxygen, aluminium and titanium are found in the spectrum, which means titanium oxide and alumina have been formed on the surface of the specimens. Similar spectra were found for other applied potential voltages. As shown in Fig. 11, the oxygen signal has decreased to zero after 1500 s sputtering in the 2 h brazed specimens applied by $E_{corr}$ potential voltage, while the signals have decreased to zero after 1800, 4500 and 6500 s sputtering in the 2 h brazed specimens applied by 1.0 V (SCE), 2.0 V (SCE), and 3.5 V (SCE), respectively. The thickness of titanium oxide (being proportional to the sputter time) of the brazed as well as the heat-treated specimens, increases with the applied potential voltages, and brazing treatment apparently exerts little effect on the kinetics of growth of the titanium oxide.

## 4. Discussion

The fatigue behaviour of titanium-based porous coating has been investigated [2–5, 8] and the values of fatigue strength are reported as 668, 394 and 141 MPa for equiaxed, non-coated lamellar, and porous-coated lamellar structures, respectively by rotating beam fatigue testing [4]. It can be concluded that the

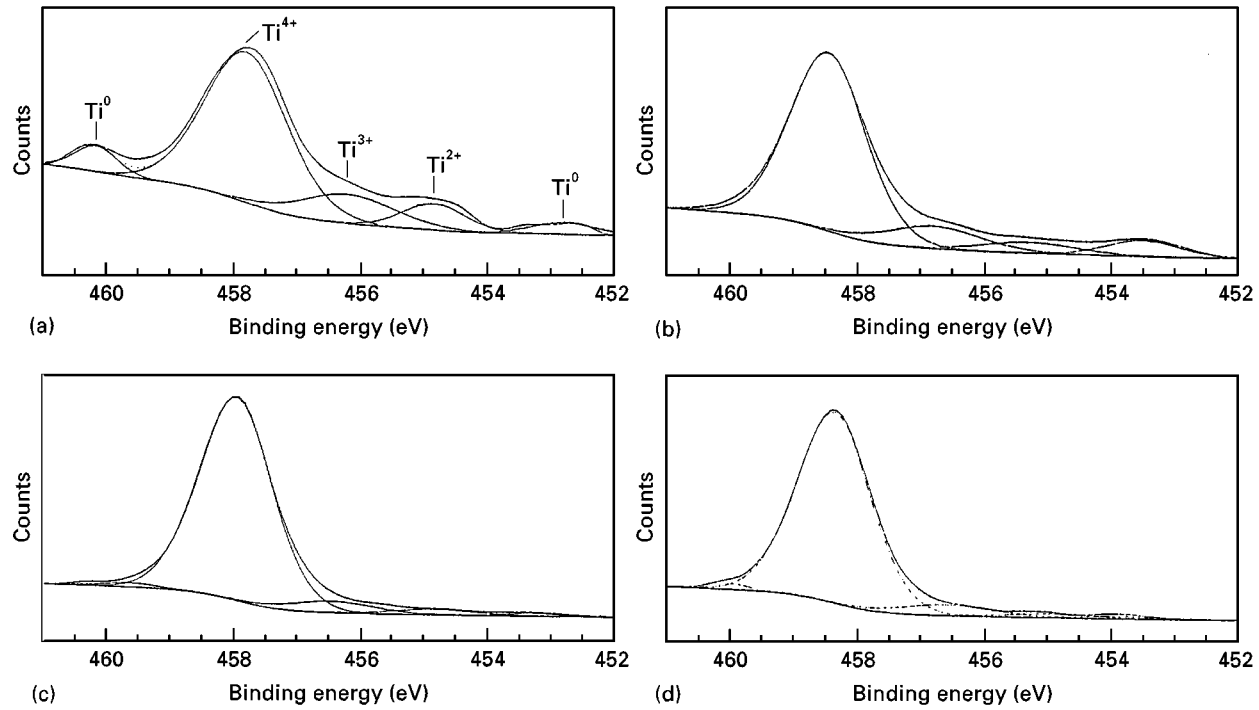


*Figure 8* Curve fit of Ti 2p spectra of HP samples under the applied potential of (a) $E_{corr}$, (b) 1.0 V (SCE), (c) 2.0 V (SCE), and (d) 3.5 V (SCE) in the potentiostatic test.

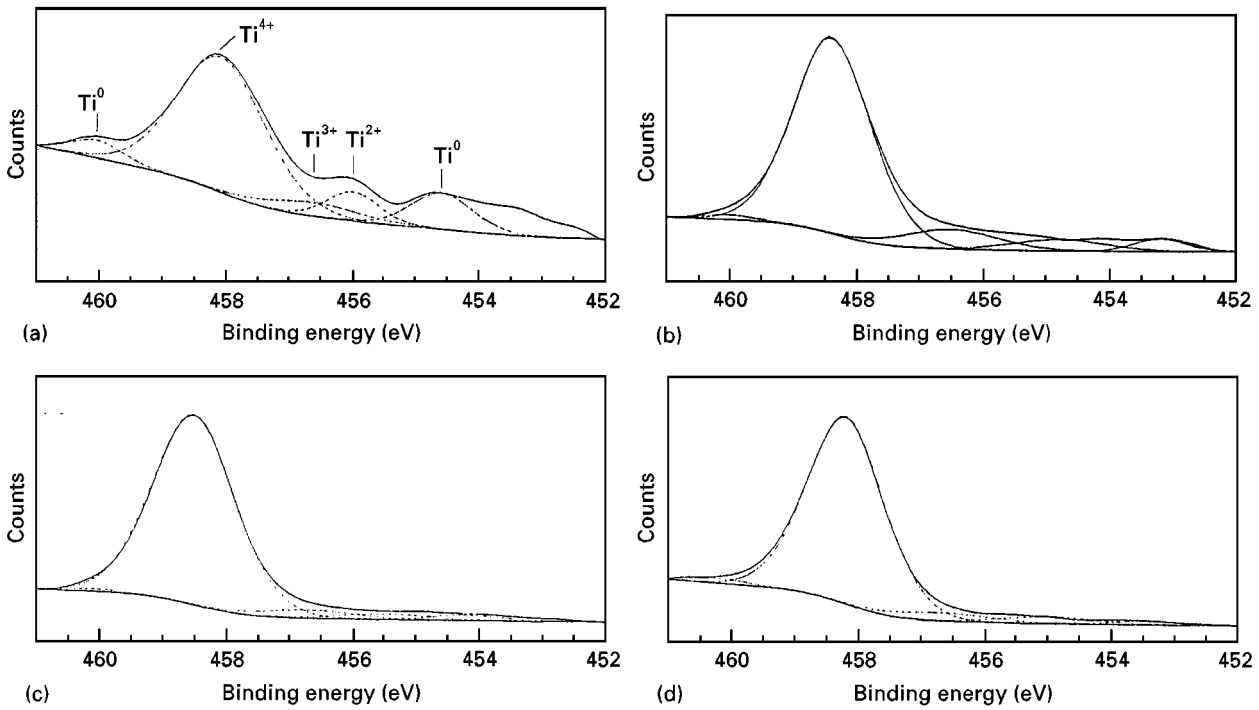


*Figure 9* Curve fit of Ti 2p spectra of B2P samples under the applied potential of (a) $E_{corr}$, (b) 1.0 V (SCE), (c) 2.0 V (SCE), and (d) 3.5 V (SCE) in the potentiostatic test.

lamellar α–β microstructure and notch effect are the two major factors which cause a significant decrease in fatigue strength. By brazing at a temperature below the beta transus temperature (992 °C), the substrate still preserves a fine equiaxed alpha grain structure and the stress concentration decreases by larger contact area and higher radius of curvature [8], which significantly improves the fatigue strength of porous-coated Ti6Al4V alloy.

Although brazing improves the fatigue strength of porous-coated Ti6Al4V alloy, it is possible that the use of titanium-based filler will decrease the corrosion resistance and accelerate the corrosion rate. The values of $I_{corr}$ of heat-treated, 2 h brazed and 8 h brazed specimens are 6.983, 7.988 and 7.632 nA $cm^{-2}$, respectively. This indicates the differences of corrosion current density, $I_{corr}$, for specimens made by the sintering method and the brazed method tend to be small.

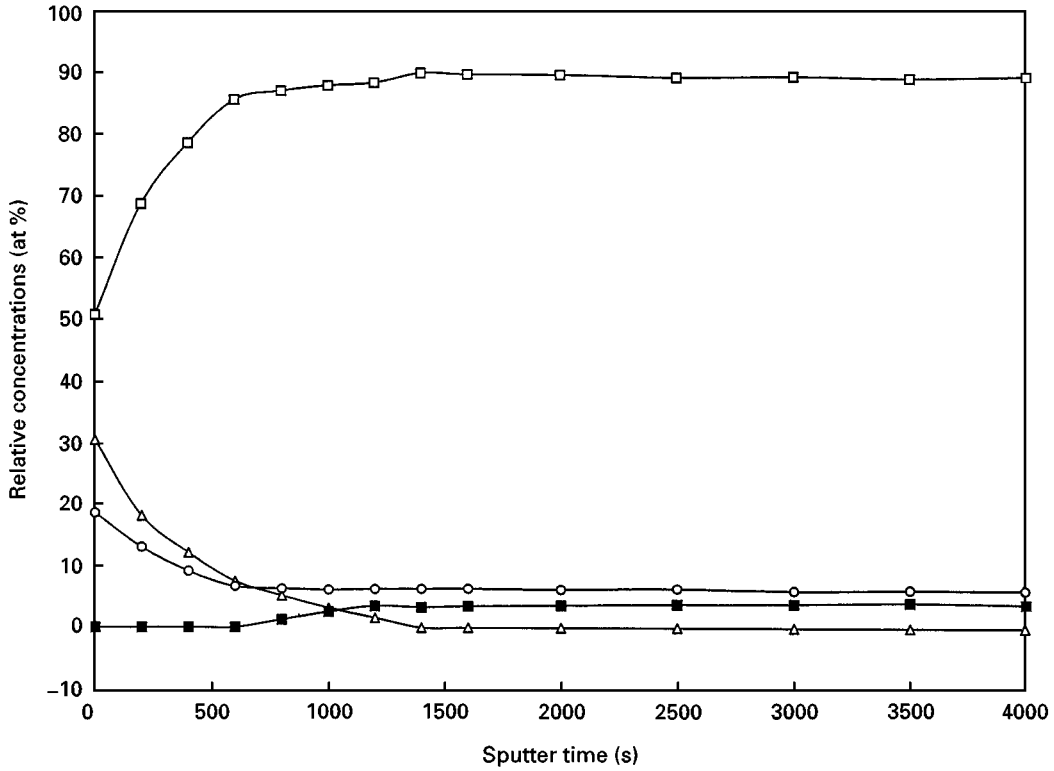


*Figure 10* Auger sputtering profiles of HP samples applied by $E_{corr}$ potential voltage in the potentiostatic test: (□) Ti, (△) O, (○) Al, (■) V.

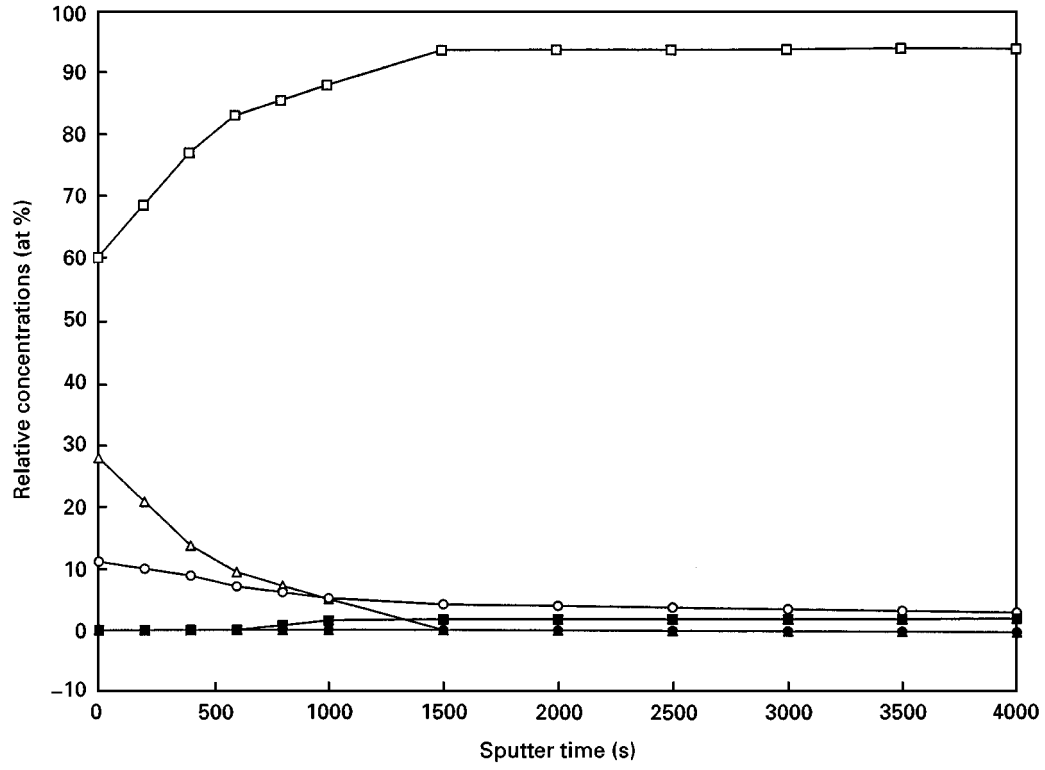


*Figure 11* Auger sputtering profiles for B2P samples applied by $E_{corr}$ potential voltage in the potentiostatic test: (□) Ti, (△) O, (○) Al, (■) V, (▲) Cu, (●) Ni.

From the XRD pattern, the quantity of $Ti_2Cu$ decreases from 2 h brazing to 8 h brazing (Fig. 1); however, the associated electrochemical corrosion analyses do not show a significant difference in the polarization curve (Fig. 2), but a slight change of corrosion potential, $E_{corr}$, can be found in Table III. The discrepancy between the results of XRD and electrochemical corrosion behaviour might be attributed to the respective depth of analyses. The behaviour of corrosion would be much affected by the composition of the nano-order surface, and similar, titanium-rich oxides as detected by XPS and AES

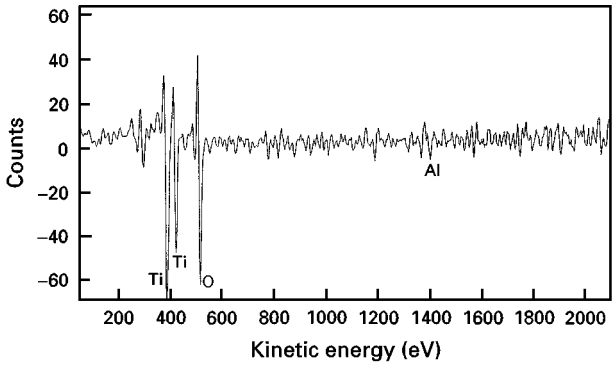


*Figure 12* AES spectrum of 500 s sputtered B2P samples subjected to $E_{corr}$ potential voltage in the potentiostatic test.

analyses for 2 h and 8 h brazed specimens were found. However, the XRD signal can be emitted from a depth more than 5 μm from the top surface.

According to the polarization curves (Fig. 2) and current density curves from the potentiostatic test (Fig. 3), the corrosion mechanism of the brazed samples is suggested to be an uniform corrosion. Although the copper- and nickel-containing brazed samples are less corrosion resistant with respect to the heat-treated samples at higher potential voltages above about 1200 mV (SCE) (Fig. 2), the passive current densities of the brazed samples are, nevertheless, lower than the heat-treated specimens at lower potential voltages. Meanwhile, the current density of the brazed samples is significantly less than the cobalt-based alloy at lower applied potential voltage. In Nielsen's study, the current density of cobalt-based alloy in Ringer's solution exceeds $10^3$ μA $cm^{-2}$ at 1.0V (SCE) in the polarization curve [9], which is supported by other research [10]. Although the existence of copper and nickel in the brazed samples slightly decreases the polarization resistance, $R_P$ (Table III), $E_{corr}$ of the brazed sample is noble to the heat-treated samples, which should be associated with the existence of copper and nickel. In the standard electromotive force potentials, the elements of copper and nickel are noble to titanium, aluminium and vanadium [11]. The existence of copper and nickel in the brazed samples promotes $E_{corr}$ in the noble direction; this explains the lower measured current density for the brazed specimens at lower potential voltage below about 1200 mV (SCE) shown in Fig. 2. A higher corrosion potential for the brazed specimen could also improve the corrosion resistance in a galvanic corrosion condition.

In the potentiostatic study, the reacted surface films of the heat-treated Ti6Al4V contain titanium, aluminium, oxygen, carbon, sodium, calcium, nitrogen and sulfur by XPS analysis where titanium and aluminium are chemical compositions in the heat-treated and the brazed samples, but oxygen, sodium, calcium and sulfur are due to the reaction with the surrounding Hank's solution during the electrochemical test. The compositions of the reacted film of the brazed samples are essentially the same as that of the heat-treated Ti6Al4V in the XPS spectra, and vanadium and brazing filler containing elements copper and nickel are not found in the spectra. In high-resolution Ti 2p spectra, the peaks are mainly composed of oxide, while suboxides and metallic components diminish rapidly with increasing applied potential in the potentiostatic tests. There are two possible reasons explaining the higher contents of $Ti^{3+}$ and $Ti^{2+}$ in the heat-treated and the brazed samples subjected to $E_{corr}$ potential. (1) Kelly has shown that titanium is oxidized to $Ti^{3+}$ in the active state and to $Ti^{4+}$ in the passive state [12]. Therefore, the existence of an active state of titanium is responsible for the higher suboxide content at $E_{corr}$. (2) According to Healy and Ducheyne [13], the shallower part of titanium oxides is predominantly composed of $Ti^{4+}$ in comparison with higher contents of $Ti^{2+}$ and $Ti^{3+}$ in the deeper part of the titanium oxides for the same Ti6Al4V sample. From the depth profile of AES in this study, the grown titanium oxide is thinner at $E_{corr}$ in comparison with higher applied potential voltages in the potentiostatic tests. Thus, the photoelectrons can survive to emanate from inner suboxides of the thinner oxide layer reacted at $E_{corr}$.

When the applied potential voltages attain 3.5 V (SCE) in the potentiostatic test, the current density of the brazed samples reaches 567.3 μA $cm^{-2}$ which is lower than the current density of 13–27 A $cm^{-2}$ during fracture and repassivation of the titanium oxide film suggested by Gilbert *et al.* [14]. The results indicate the brazed samples are stable and passive in the electrochemical tests, and the oxide film is predominantly composed of titanium oxide which is the same as the heat-treated samples.

Auger profiles of both heat-treated and brazed samples from the potentiostatic test show that titanium increases monotonically to constant values for all the applied potential voltages, and aluminium continuously decreases to constant values during the depth profile examination (Figs 10 and 11). The enrichments of aluminium are observed in the outermost surface of the reacted films of both brazed and heat-treated samples. The higher contents of aluminium were also observed by several researchers [15, 16]. Ask *et al.* [17] have investigated the anodic oxides of Ti6Al4V and found a relatively high atomic concentration of aluminium (Al/Ti = 0.17) for Ti6Al4V anodized in $H_2SO_4$ at 45 V. By depth profile of AES in the present study, the contents of aluminium of the brazed samples were found to be lower than the heat-treated samples, which must be caused by the difference in initial compositions of the unreacted samples before the potentiostatic test. By EDS analyses (Table II), the brazed sample is shown to have a lower content of aluminium in comparison with the heat-treated samples, thus lower concentrations of aluminium ions are found to be released from the brazed specimens in comparison with the heat-treated samples in simulated body fluid [18].

The reacted surface films of the brazed specimens from the electrochemical corrosion test are mainly composed of titanium oxide as found by XPS and AES analyses, being the same as the heat-treated samples. Meanwhile, copper and nickel are not detected

by AES and XPS analysis, suggesting that they are not in contact with the surrounding Hank's solution. Therefore, the formation of titanium-rich oxide, containing less alumina and no copper and nickel elements in the surfaces of the brazed specimens, might be deduced to perform as well as the heat-treated Ti6Al4V *in vivo* test. Whether the potentially lower ion release of aluminium to the physiological environment is significant, needs to be studied.

## 5. Conclusions

Work was carried out to compare the electrochemical properties and surface characteristics of the brazed and the heat-treated Ti6Al4V in Hank's soluion. The results from this study can be summarized as follows.

1. In the potentiodynamic test, the corrosion rates of the heat-treated and the brazed samples are similar at $E_{corr}$, and the value of $E_{corr}$ for the brazed sample is found to be noble to the heat-treated samples. The passive current density of the brazed specimen is either lower or higher than the heat-treated specimen, depending on the polarization potential.

2. By AES and XPS analysis on specimens from the potentiostatic test, the reacted surface films of the heat-treated and the brazed specimens from electrochemical test are found to be mainly composed of titanium oxide, and the thickness of the titanium oxide for both specimens increases with increasing applied potential voltages. The elements of copper and nickel in the brazing filler are not detected, while less alumina is found in the reacted film of the brazed specimens as compared with the heat-treated specimens.

## References


1. S. LAMPMAN, in "Metals Handbook" Vol. 2, edited by J.R. Davis, P. Allen, S. R. Lampman, T. B. Zorc, J. L. Daquila, A. W. Ronke, J. Jakel, K. L. O'keefe and R. L. Stedfeld (ASM International, Materials Park, OH, 1990) p. 592.
2. S. YUE, R. M. PILLAR and G.C. WEATHERLY, *J. Biomed. Mater. Res.* **18** (1984) 1043.
3. S. D. COOK, F. S. GEOGETTE, H. B. SKINNER and R. J. HADDAD, *ibid.* **18** (1984) 497.
4. S. D. COOK, N. THOMGPREDA, R.C. ANDERSON and R.J. HADDAD, *ibid.* **22** (1988) 287.
5. C. A. STUBBINGTON and A.W. BOWEN, *ibid.* **9** (1974) 941.
6. C. D. BUGLE, US Pat. 4854 496 (1989).
7. C. CRIVELLA and L.A. STOUSE, US Pat. 4650 109 (1987).
8. C.H. YEN, Master Thesis, National Cheng Kung University, Tainan, Taiwan (1995).
9. K. NIELSEN, *Br. Corros. J.* **22** (1987) 272.
10. Y. NAKAYAMA, T. YAMAMURO, Y. KOTOURA and M. OKA, *Biomaterials* **10** (1989) 420.
11. A. J. deBETHUNE and N. S. LOUD, "Standard Electrode Potentials and Temperature Coefficients at 25 °C", (Clifford A. Hampet, Skokie IL, 1964).
12. E. J. KELLY, in "Modern Aspects of Electrochemistry No. 14", edited by J.O'M. Bockris, B.E. Conway and R.E. White (Plenum Press, NewYork, 1982) p. 319.
13. K. E. HEALY and P. DUCHEYNE, *J. Biomed. Mater. Res.* **26** (1992) 319.
14. J. L. GILBERT, C. A. BUCKLEY and E.P. LAUTENSCHLAGER, in "Medical Applications of Titanium and Its alloys: The Material and Biological Issues", edited by S.A. Brown and J.E. Lemons (American Society for Testing and Materials, Philadelphia, PA, 1996) p. 199.
15. D.C. SMITH, R.M. PILLAR and R. CHERNECKY, *J. Biomed. Mater. Res.* **25** (1991) 1045.
16. D. C. SMITH, R. M. PILLAR, J. B. METSON and N. S. MCINTYRE, *ibid.* **25** (1991) 1069.
17. M. ASK, L. LAUSMMA and B. KASEMO, *Appl. Surf. Sci.* **35** (1988) 283.
18. T. M. LEE, E. CHANG and C. Y. YANG, unpublished data (1997).



*Received 9 June*
*and accepted 16 September 1997*